JOURNAL OF COMPUTATIONAL PHYSICS 116, 143–153 (1995)

Alternate Formulations for the Pressure Equation Laplacian on a Collocated Grid for Solving the Unsteady Incompressible Navier–Stokes Equations

DANESH TAFTI

National Center for Supercomputing Applications, University of Illinois at Urbana/Champaign, Urbana, Illinois 61801

Received September 8, 1993; revised March 31, 1994

The solution of the unsteady incompressible Navier–Stokes on a collocated grid is investigated. A consistent formulation to construct the Laplacian in the pressure equation is developed. It is shown that within this framework, Laplacians with different characteristics can be constructed, which can be made to satisfy discrete continuity and considerably reduce pressure oscillations. A third-order forward-biased approximation for the gradient operator of pressure works very well in completely eliminating pressure oscillations in a lid-driven cavity flow test problem.

1. INTRODUCTION

The accurate numerical solution of the incompressible Navier–Stokes equations has been the subject of much research. A commonly used method is the artificial compressibility method [1] in which the continuity equation is solved by adding an artificial pressure time derivative. In the other class of methods, the continuity equation is used to derive an elliptic pressure–Poisson equation. The pressure–Poisson equation is either derived from the continuum equations directly [2] and then discretized or more commonly it is derived from the discretized form of the continuum equations [3]. The SIMPLE based algorithms [4] and the "time-split or fractional-step methods" [3] fall under this later category. In both of these last algorithms, the calculated pressure (correction) is used to correct an intermediate velocity field to make it divergence free. The staggered grid approach, where the velocity and pressure are displaced by $\Delta/2$ in space, used in conjunction with a finite-volume formulation provides an effective way to solve the set of equations. This approach is particularly useful in solving the pressure–Poisson equation and satisfies both, discrete continuity to machine accuracy and, also, the physical requirement of a smooth oscillation-free pressure field. However, the staggered nature of the grid introduces considerable complexity and increased memory requirements in the bookkeeping aspects of the grid. These restrictions are particularly severe in problems with complex geometries when used in conjunction with high-order finite difference approximations and in applications with unstructured grids and adaptive grid refinement.

Collocated grids (all variables are calculated at the same location in space), on the other hand, provide geometrical simplicity when dealing with complex calculation domains and algorithms. Unfortunately, collocated grids pose difficulties in satisfying continuity exactly and/or introducing unphysical grid scale oscillations in the calculated pressure field. It is not surprising that the formulation of the pressure equation has a direct bearing on these two issues, the resolution of which have been extensively studied by researchers (Strikwerda [5], Bube and Strikwerda [6], Sotiropoulos and Abdallah [7]). Two important issues in the formulation of the pressure equation are its "regularity" and its "integrability" (Strikwerda [5], Armfield [8]). Regularity is a measure of the discrete Laplacian's ability to accurately represent all the wavenumbers as dictated by the ellipticity of the continuous Laplacian operator. The inability of the discrete operator to resolve the high wavenumbers, in particular the grid scales (non-dimensional wavenumber of π), leads to grid scale oscillations in the pressure field.

In the staggered grid system the Laplacian of pressure utilizes the stencil $(i - 1, i, i + 1)$ (since the subject of this paper is the construction of the Laplacian in the pressure equation, for convenience the one-dimensional second derivative will be referred to as the Laplacian in all the text that follows) and in Fourier space it has no zeros in the range $(0, \pi)$ and resolves the high wavenumbers with good accuracy. However, on a collocated grid with a finite-volume formulation, the Laplacian utilizes the stencil $(i - 2, i, i + 2)$ (see, for example, Chorin [3]). Fourier analysis shows that it does not resolve the high wavenumbers with good accuracy and completely fails to resolve the grid scales (non-dimensional wavenumber π). Rhie and Chow [9] have formulated the SIMPLE algorithm on a collocated grid. Their formulation on the collocated grid closely mimicked the staggered grid formulation by using a momentum-based interpolation for the cell face velocities in the continuity equation. Consequently, their Laplacian was of type $(i - 1, i, i + 1)$ and did not have problems with oscillating grid scales. Strikwerda [5] and Strikwerda and Nagel [10] use what they call "regularizing terms" in the gradient and divergence operators to construct the Laplacian. These regularizing terms

0021-9991/95 $6.00

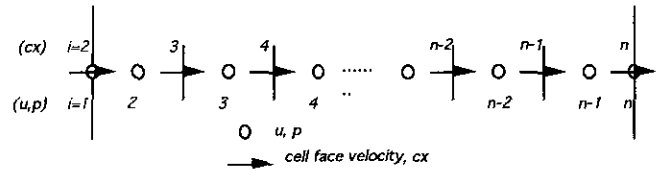

FIG. 1. Equivalent one-dimensional collocated grid topology.

increase the resolution at high wavenumbers and the grid scales to eliminate pressure oscillations. However, as a consequence of this they are unable to satisfy discrete continuity. Similarly, Sotiropoulus and Abdallah [7], have elucidated on the dilemma of trying to satisfy continuity and at the same time eliminate the pressure oscillations. By discretizing the continuum pressure–Poisson equation, they have shown that by using a $(i-1, i, i+1)$ stencil for the Laplacian on a collocated grid, the pressure oscillations are eliminated; however, discrete continuity has errors proportional to the fourth-order spatial derivatives of the pressure and velocity components. On the other hand, by deriving the pressure–Poisson equation from the discrete continuity equation, the Laplacian is of the form $(i-2, i, i+2)$, which satisfies discrete continuity but introduces pressure oscillations. They have suggested a compromise; by the addition of fourth-order spatial derivative regularizing terms to the $(i-2, i, i+2)$ Laplacian of pressure. By numerical experiments they found that relatively small contributions from the regularizing terms avoided the pressure oscillations. However by doing so, discrete continuity was not satisfied exactly. In a recent study, Najjar and Vanka [11] have studied the effect of using different high-order approximations to the pressure–Poisson equation on a collocated grid. They used finite-difference and finite-volume discretizations for the Laplacian. Their study shows that the finite-difference approximations do not satisfy discrete continuity and also do not satisfy the integrability constraint.

The integrability constraint [12] states that the solution to the pressure–Poisson equation with Neumann boundary conditions exists only if the discretized form satisfies certain conditions. On a staggered grid with a finite-volume formulation two discretized forms need to be satisfied,

$$\int_V \nabla \cdot \mathbf{u}\, dv = \int_S \mathbf{u} \cdot d\mathbf{S} \tag{1}$$

$$\int_S \nabla p \cdot d\mathbf{S} = \frac{1}{\Delta T}\int_S \mathbf{u} \cdot d\mathbf{S}, \tag{2}$$

where, $d\mathbf{S} = \mathbf{n}dS$, $\mathbf{n}$ is the unit outward normal to the surface encompassing the computational domain, and dS is the grid spacing. The first condition states that the global volume weighted summation of the divergence operator must reduce to a statement of global mass conservation at the computational boundaries. In a finite-volume staggered mesh system, the normal derivative of pressure ($\nabla p \cdot d\mathbf{S}$) is set to zero at the boundaries. This is a consequence of the finite-volume formulation and the fact that the velocity at the boundary is assumed to be known and does not require a pressure correction. As shown by Gresho and Sani [13], this is equivalent to applying the Neumann boundary condition in terms of the normal viscous stresses to the pressure node adjacent to the boundary. Hence, if the discrete divergence operator can be reduced from a volume integral summed over the whole domain to a surface integral at the boundaries and if global continuity is satisfied, then the formulation of the pressure–Poisson equation satisfies integrability. In the present work the topology of the collocated grid closely resembles that of the staggered grid, and similar conditions need to be met to satisfy the integrability constraint.

In this paper the implementation of the fractional-step method for the unsteady incompressible Navier–Stokes equations on a collocated grid is described. The main objective of the present work is to develop and apply a consistent formulation for the Laplacian in the pressure equation on a collocated grid. Different forms of the Laplacian are derived. Fourier analysis and the application to a model-driven cavity problem are used to evaluate the effectiveness of different formulations. The most important contribution of this work is in the introduction of a framework within which Laplacians can be constructed which considerably reduce or eliminate pressure oscillations and at the same time satisfy discrete continuity exactly. In time integration algorithms, local mass conservation plays an important role in avoiding spurious production of energy and vorticity which can pollute the velocity field and in extreme cases can lead to instabilities [14]. Also, when using high-order finite difference approximations with truncation errors of order $\Delta^{3,5}$ and upwards, it is important to satisfy local continuity to maintain the overall high order of accuracy [11].

2. GOVERNING EQUATIONS AND COLLOCATED GRID TOPOLOGY

The time-dependent, non-dimensionalized, incompressible continuity and momentum equations are of the form

$$\frac{\partial u_i}{\partial x_i} = 0 \tag{3}$$

$$\frac{\partial u_i}{\partial T} + \frac{\partial}{\partial x_j}(u_i u_j) = -\frac{\partial p}{\partial x_i} + \frac{1}{\mathrm{Re}}\frac{\partial^2 u_i}{\partial x_j^2}, \tag{4}$$

where $i = 1, 2, 3$ corresponds to x (u), y (v), and z (w) coordinates (velocities) in three dimensions and Re is the Reyn-

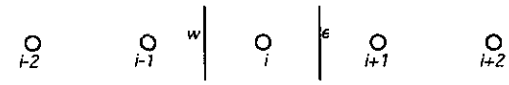

FIG. 2. Equivalent one-dimensional finite-volume for divergence operator.

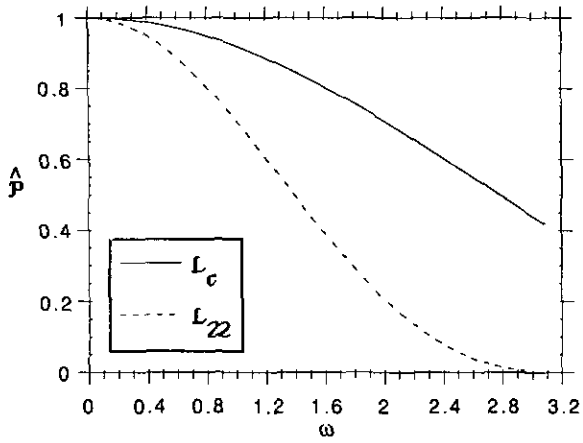

FIG. 3. Variation of normalized Fourier coefficients $\hat{\mathcal{P}}$ for $\mathcal{L}_c$ and $\mathcal{L}_{22}$ with nondimensional wavenumber ω.

olds number. These equations are solved on a collocated grid. The grid topology is similar to that used in the staggered grid system with the exception that the primary flow variables are solved at the same location in space. Figure 1 shows a representative grid for the x-direction. The velocity u and pressure p are solved from $i = 2, n - 1$. The cell face velocities (cx) are calculated from $i = 2, n$. They represent the mass flux entering and leaving the finite-volume surrounding the velocity and pressure node. The cell face velocity is interpolated using the velocity u at surrounding nodes and is used in the calculation of the convection terms in the momentum equations and also in calculating the mass source term in the pressure–Poisson equation.

3. NUMERICAL ALGORITHM AND PROBLEMS WITH THE PRESSURE–POISSON EQUATION

In the fractional-step method (Chorin [3], Harlow and Welch [15], Kim and Moin [16]), an intermediate velocity field ($\tilde{u}_j$) (j is used as a vector notation) is calculated, either by completely neglecting the contribution of the pressure gradient to momentum balance or by using the pressure field from the previous time step (p^n). In either case, the intermediate velocity field is made divergence free (u_j^{n+1}) by solving a pressure–Poisson equation. In the present study a second-order explicit Adams–Bashforth scheme is used to advance the solution in time for both the convection and the viscous terms. Symbolically, these steps can be represented by the equations

$$\frac{\tilde{u}_j - u_j^n}{\Delta T} = \frac{3}{2} H_j^n - \frac{1}{2} H_j^{n-1}, \tag{5}$$

where $\tilde{u}_j$ denotes the intermediate velocity field and

$$H_j = -\frac{\partial}{\partial x_k}(u_j u_k) + \frac{1}{\mathrm{Re}} \frac{\partial^2 u_j}{\partial x_k^2}. \tag{6}$$

In calculating the convection terms, the interpolated cell face velocities (cx, cy, cz) are used to calculate the mass fluxes across the finite-volume. The momentum velocities at the cell faces are obtained by using second-order central differencing and the viscous terms are also second-order accurate. It should be noted that the implementation of the first step on a collocated grid does not require any special considerations. In fact, as stated in the Introduction, the calculation of the grid metrics is considerably simplified since the same finite-difference coefficients can be used for all three components of velocity.

In the second step the velocity ($\tilde{u}_j$) is corrected to satisfy Eqs. (3) and (4) at $T = (n + 1)\,\Delta T$ to give u_j^{n+1}:

$$u_j^{n+1} = \tilde{u}_j - \Delta T \frac{\partial p^{n+1}}{\partial x_j}. \tag{7}$$

The formulation of the pressure equation is crucial to both the accuracy of the pressure field and the satisfaction of discrete continuity. With reference to Fig. 2, the divergence operator in Eq. (3) can be discretized in a finite-volume sense and can be written in terms of fluxes entering and leaving the west and east faces (in 1D). This approximation is of second-order accuracy on a uniform grid. Other approximations to the divergence operator would be to abandon the finite-volume approach in the interests of high-order accurate approximations [17]. However, as found in [17], the use of high-order approximations in the form of a fourth-order central difference operator does not satisfy the integrability constraint exactly and is prone to artificial mass sources and sinks in the calculated velocity field. Hence, in the present work, the control-volume approach which is second-order accurate in space is used for the divergence operator. It should be pointed out that by opting to use this approximation for the divergence operator, many of the problems associated with satisfying discrete continuity are elimi-

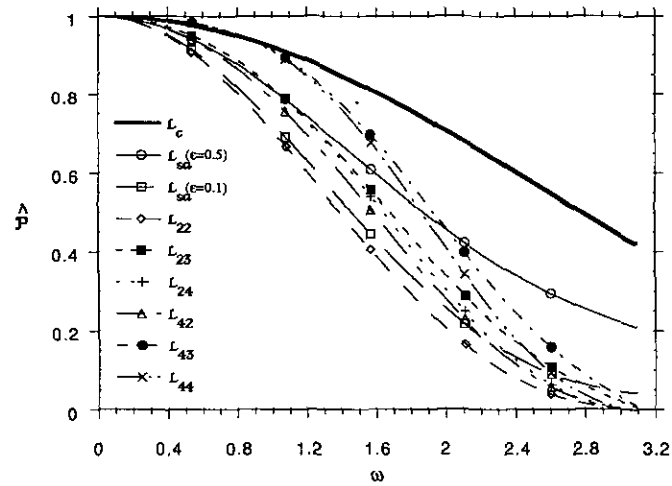

FIG. 4. Variation of normalized Fourier coefficients $\hat{\mathcal{P}}$ with non-dimensional wavenumber ω for different Laplacians.

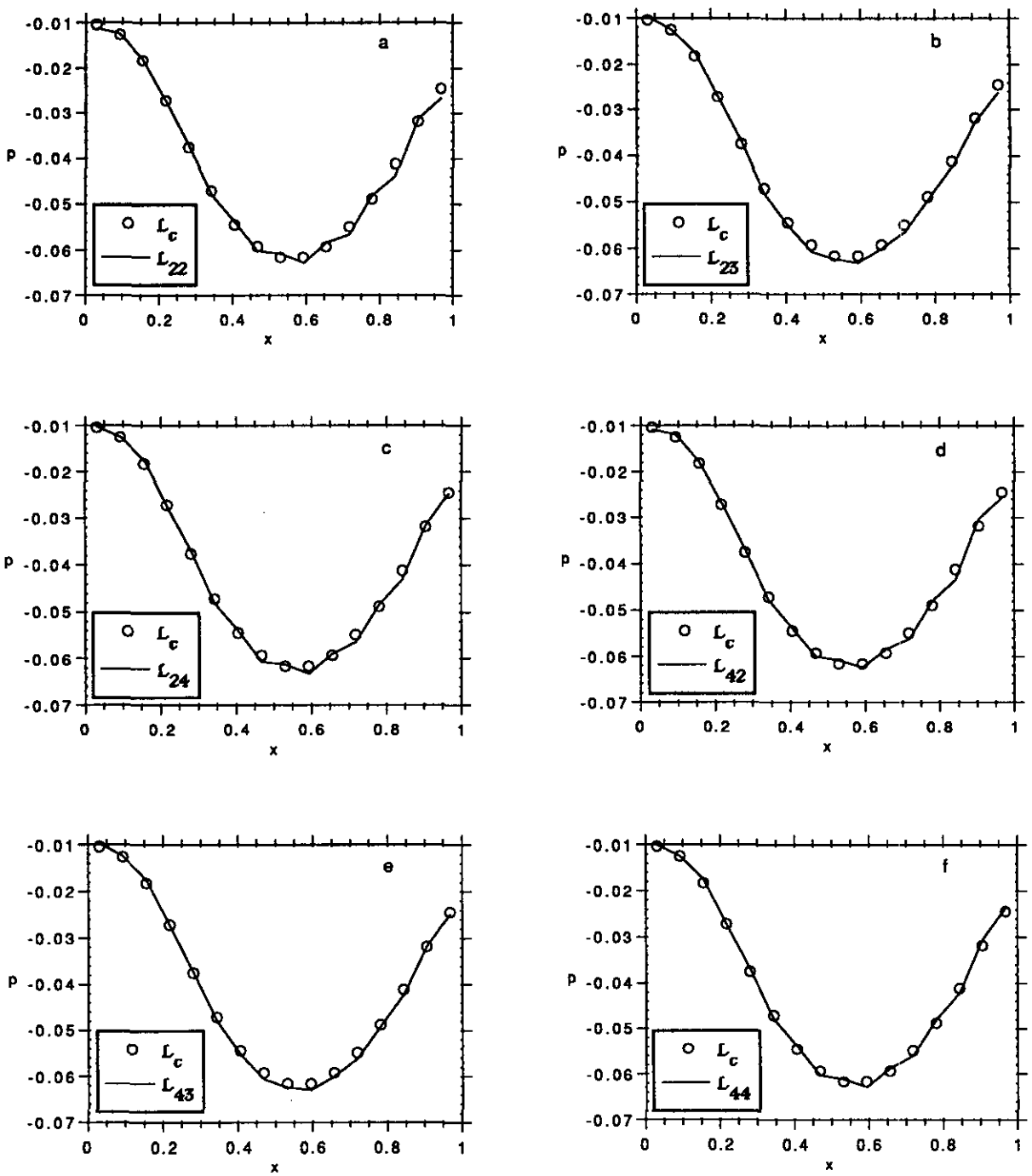

FIG. 5. Calculated pressure field at $y = 0.5$ for a driven cavity problem at Re = 1000 and 16 × 16 computational cells. $\mathcal{L}_c$ is the compact Laplacian corresponding to a staggered grid calculation.

nated. Based on this approximation, the one-dimensional discrete continuity equation is written as

$$\frac{u\big|_e^{n+1} - u\big|_w^{n+1}}{\Delta} = 0. \tag{8}$$

From Eq. (7), the cell face velocities can be represented by

$$u_{(e,w)}^{n+1} = \tilde{u}_{(e,w)} - \Delta T \frac{\partial p}{\partial x}\bigg|_{(e,w)}^{n+1}. \tag{9}$$

On a staggered grid system, Eq. (9) does not pose any problem because $\tilde{u}_{(e,w)}$ and the pressure gradient operator are available at the cell faces (location of u-velocity nodes) of the pressure

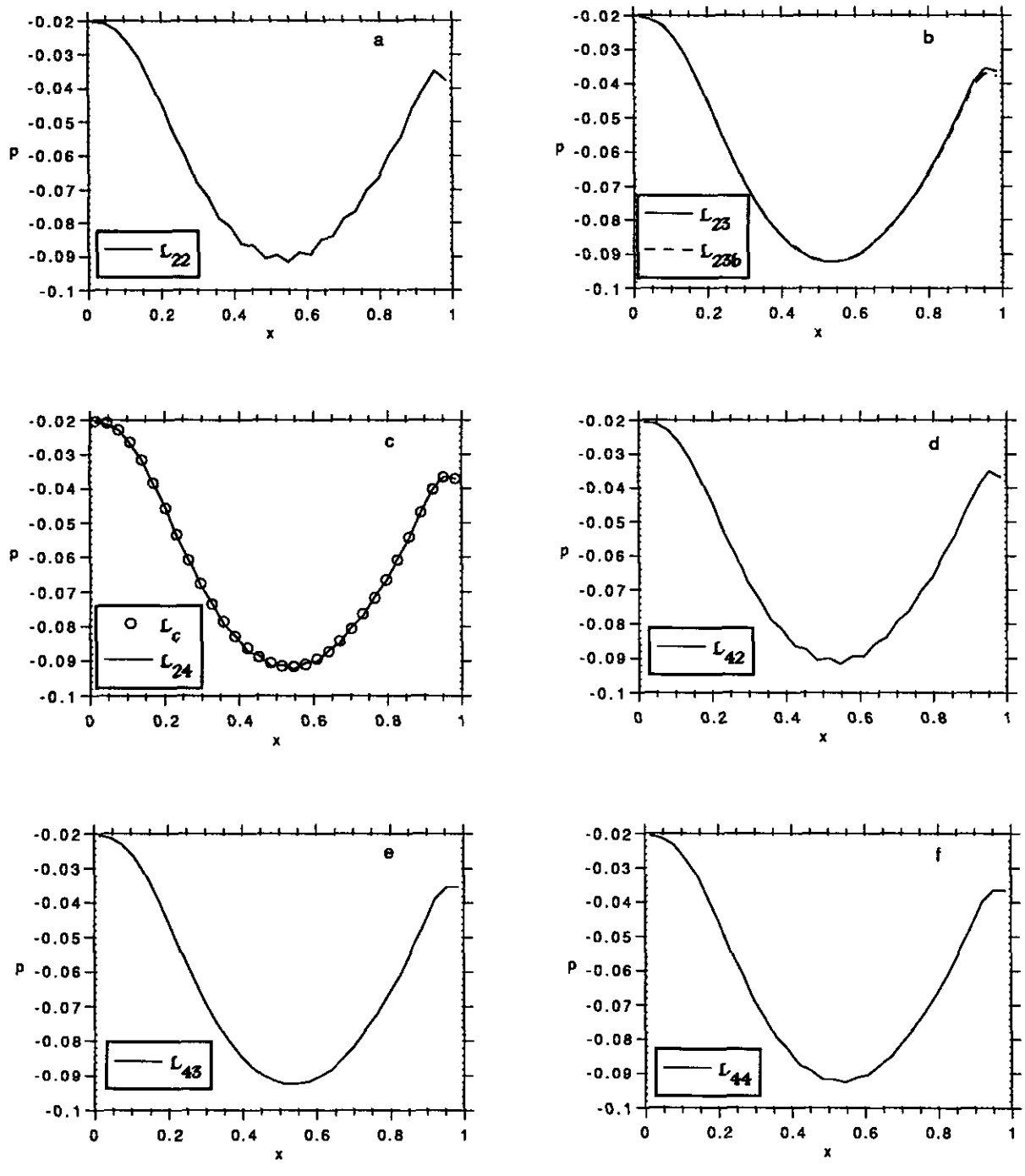

FIG. 6. Calculated pressure field at $y = 0.5$ for a driven cavity problem at Re = 1000 and 32 × 32 computational cells. $\mathcal{L}_c$ is the compact Laplacian corresponding to a staggered grid calculation.

node and no approximations are needed in evaluating these terms. This is not true for the collocated grid, where both terms in Eq. (9) have to be approximated at the cell faces. One way to do this would be to interpolate the cell face velocities ($\widetilde{cx}$, $\widetilde{cy}$, $\widetilde{cz}$) from the neighboring nodes and approximate the pressure gradient term directly. As an example, Eq. (9) for the east cell face would reduce to

$$u_e^{n+1} = \widetilde{cx}_e - \Delta T \frac{p_{i+1}^{n+1} - p_i^{n+1}}{\Delta}. \tag{10}$$

The gradient operator in Eq. (10) is second-order accurate in space on a uniform grid. Substituting Eq. (10) (and a similar approximation for the west face) into Eq. (8), the Laplace operator for the pressure–Poisson equation is of the same com-

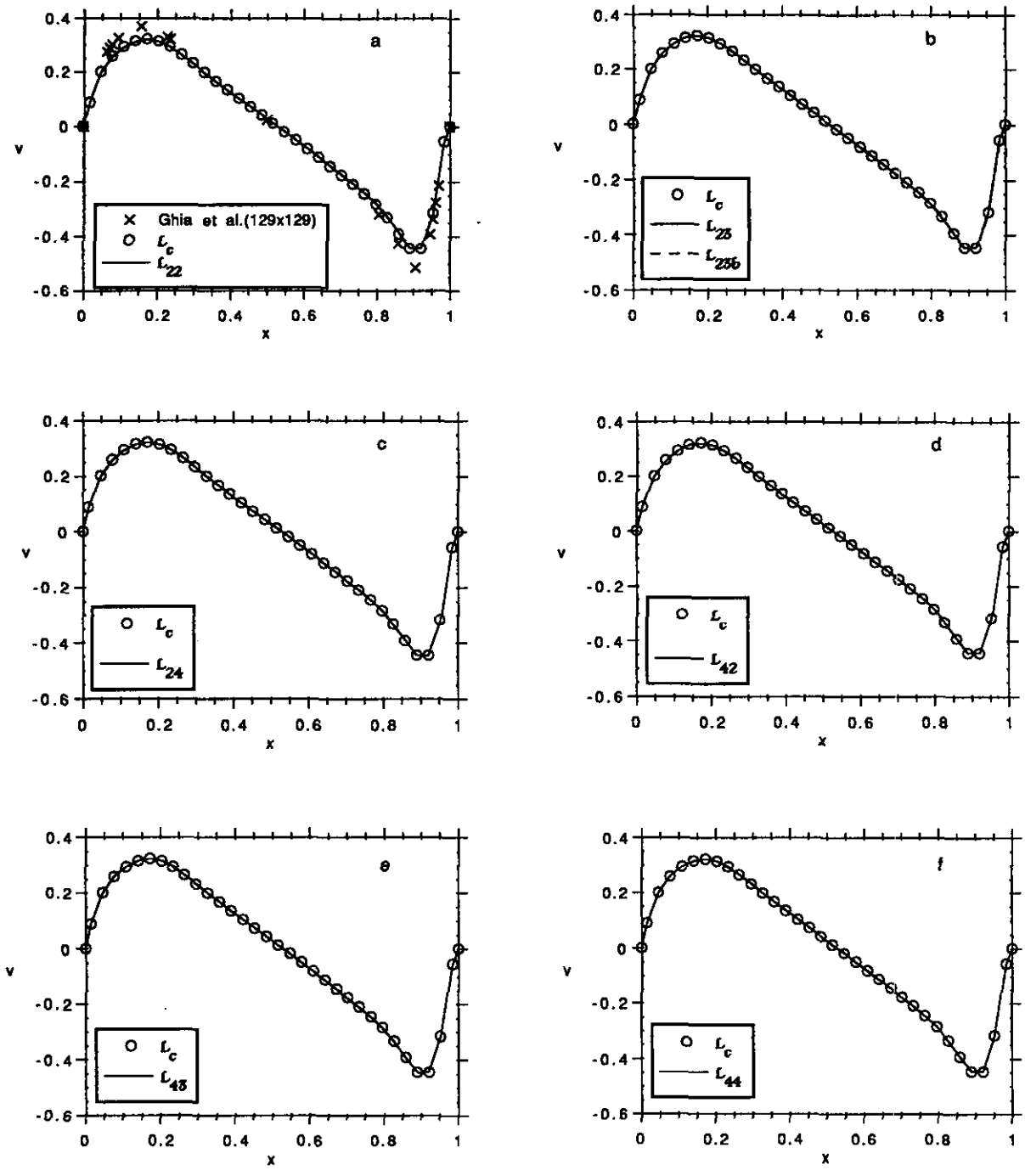

FIG. 7. Calculated velocity field at $y = 0.5$ for a driven cavity problem at Re = 1000 and 32 × 32 computational cells. $\mathcal{L}_c$ is the compact Laplacian corresponding to a staggered grid calculation.

pact form $(i - 1, i, i + 1)$ as one would obtain on a staggered grid. Consequently, this does not introduce any spurious oscillations in the calculated pressure field. However, this formulation does not satisfy discrete continuity exactly and has been discussed at some length by Sotiropoulus and Abdallah [7]. The approximation of the pressure gradient term in Eq. (9) is inconsistent with that applied to the velocity nodes and during the correction phase (Eq. (7)) this inconsistency creates artificial mass sources and sinks. According to Sotiropoulus and Abdallah [7], the error introduced is proportional to the fourth spatial derivative of pressure and velocity.

A more consistent approach to the approximation of Eq. (9) is to apply the same interpolation operator to the pressure gradient term as used to calculate the cell face velocities ($\widetilde{cx}$, $\widetilde{cy}$,

TABLE I

Summary of Laplacians on a Uniform Grid

	$i-4$	$i-3$	$i-2$	$i-1$	i	$i+1$	$i+2$	$i+3$	$i+4$
$\mathscr{L}_{22} \times 4\Delta^2$	—	—	1	0	−2	0	1	—	—
$\mathscr{L}_{23} \times 12\Delta^2$	—	—	2	3	−8	−2	6	−1	—
$\mathscr{L}_{24} \times 24\Delta^2$	—	−1	8	1	−16	1	8	−1	—
$\mathscr{L}_{42} \times 32\Delta^2$	—	−1	10	1	−20	1	10	−1	—
$\mathscr{L}_{43} \times 96\Delta^2$	—	−2	17	36	−81	−18	63	−16	1
$\mathscr{L}_{44} \times 192\Delta^2$	1	−18	80	18	−162	18	80	−18	1

$\widetilde{cz}$). For example, for a second-order accurate central-difference interpolation operator used to calculate $\widetilde{cx}_e$, the pressure gradient on the east face is calculated as

$$\left.\frac{\partial p}{\partial x}\right|_e^{n+1} = \frac{1}{2}\left\{\left.\frac{\partial p}{\partial x}\right|_i^{n+1} + \left.\frac{\partial p}{\partial x}\right|_{i+1}^{n+1}\right\}. \tag{11}$$

Substituting Eq. (9) into Eq. (8) and using the approximation for the pressure gradient at the cell face implied by Eq. (11), we can obtain the one-dimensional equivalent of the pressure–Poisson equation. In this approach if the pressure gradient is approximated using second-order accurate central-differences on a uniform grid, then the Laplacian has the form ($i-2$, i, $i+2$). This form of the Laplacian has a very weak representation in the high wavenumber region and introduces grid scale oscillations in the pressure field. However, because of the consistent treatment of the pressure gradient term in Eq. (7), discrete continuity is satisfied exactly.

We have found that by using two different approaches in approximating the cell face pressure gradient term in Eq. (9), the first gives a correct pressure field but does not satisfy discrete continuity and the other satisfies continuity but gives an oscillating pressure field. The purpose of this paper is to show alternate methods of constructing Laplacians which can be made to satisfy discrete continuity and at the same time considerably reduce, or in some cases, eliminate pressure oscillations.

To further develop the methodology and the rationale, it is instructive to look at the Fourier representation of the two Laplacians derived above. For completeness, the two Laplacians are given by

$$\mathscr{L}_c = \frac{p_{i+1} - 2p_i + p_{i-1}}{\Delta^2} \tag{12}$$

$$\mathscr{L}_{22} = \frac{p_{i+2} - 2p_i + p_{i-2}}{4\Delta^2}, \tag{13}$$

where $\mathscr{L}$ is the Laplacian and c represents the "compact form," while 22 stands for a second-order interpolant and second-order accurate gradient operator, respectively.

The discrete Fourier representation of a real variable p can be written as

$$p(x_j) = \sum_{k=0}^{N/2} \hat{p}(k) e^{ikx_j}, \tag{14}$$

where $\hat{p}$ are the Fourier coefficients for each wavenumber k, and $x_j = 2\pi j/N$ are the collocation points. Applying Eq. (14) to the discrete Laplacians in Eqs. (12) and (13) and then normalizing by the exact representation of the continuous Laplacian in Eq. (14), we can obtain the normalized Fourier coefficients for the discrete Laplacians. The normalized coefficients for Eqs. (12) and (13) are given by

$$\hat{\mathscr{P}}_c(\omega) = -\frac{2}{\omega^2}\{\cos(\omega) - 1\} \tag{15}$$

and

$$\hat{\mathscr{P}}_{22}(\omega) = -\frac{1}{2\omega^2}\{\cos(2\omega) - 1\}, \tag{16}$$

where $\omega = k\Delta$ is a non-dimensional wavenumber and varies from $(0, \pi)$. Figure 3 plots the variation of $\hat{\mathscr{P}}_c$ and $\hat{\mathscr{P}}_{22}$ against the wavenumber. A value of $\hat{\mathscr{P}}$ near unity in wavenumber space indicates an accurate representation of the ellipticity of the continuous Laplacian by the discrete approximation. The most striking difference between the Fourier coefficients of the two Laplacians is the much better accuracy/ellipticity exhibited by the compact formulation in wave space. The difference between the two increases in the high-wavenumber region, where $\mathscr{L}_{22}$ completely fails to resolve the grid scales ($\omega = \pi$). Having observed this difference in behavior between the two cases, the question follows whether it is possible to construct a Laplacian which will approach the behavior of the compact formulation and at the same time satisfy discrete continuity? And, if this is to be achieved, is it mandatory to resolve the grid-scale ($\omega = \pi$), or will increased resolution in the mid-high wavenumber range suffice to damp the pressure oscillations? The rest of the paper will address these issues by evaluating alternate formulations of the Laplacian in the pressure equation. How-

ever, before we proceed any further, it would be helpful to formalize a general basis for the construction of the Laplacian.

4. ALTERNATE FORMULATIONS OF THE LAPLACIAN

Equation (9) can be re-written as

$$u^{n+1} = \{\mathcal{I}\}\tilde{u} - \Delta T\{\mathcal{I}\mathcal{G}\}p \tag{17}$$

where $\mathcal{I}$ is the discrete interpolation operator and $\mathcal{G}$ is the discrete gradient operator. Applying the discrete divergence operator ($\mathcal{D}$) to Eq. (17) we can write the pressure–Poisson equation as

$$[\mathcal{D}\mathcal{I}\mathcal{G}]p = \frac{1}{\Delta T}[\mathcal{D}\mathcal{I}]\tilde{u}, \tag{18}$$

where the Laplacian $\mathcal{L} = [\mathcal{D}\mathcal{I}\mathcal{G}]$. By using different finite-difference formulations for the three operators which comprise the Laplacian we can manipulate its properties. In the present work the $\mathcal{D}$ operator is assumed to be of the form implied in Eq. (8). As stated previously, the finite-volume approximation in Eq. (8), although just second-order accurate, has very desirable properties regarding satisfying the integrability constraint [17] and consequently discrete continuity. On the other hand, the approximation of the discrete $\mathcal{I}$ and $\mathcal{G}$ operators do not have any direct bearing on the integrability constraint and give us the opportunity to explore different forms and their subsequent effect on the ellipticity of the discrete Laplacian. It should be stated that all the Laplacians constructed in this manner have second-order accuracy at best.

4.1. *The Gradient Operator* ($\mathcal{G}$)

Three forms of the gradient operator $\mathcal{G}$ are investigated in the present work. A second-order accurate central-difference form, a third-order forward-biased form, and a fourth-order central-difference form. It should be noted that a reverse biasing (backward) has a similar effect on the constructed Laplacian. For simplicity, each approximation is treated separately in its one-dimensional form on a uniform grid. These operators are applied to the velocity nodes 2 through $n - 1$ (see Fig. 1). For completeness the boundary approximations are also given. Nodes 1 and n are not included in the boundary approximations and, correspondingly, one-sided differences are used in such instances.

Second-order central-difference:

$$\text{Interior, } 3 \le i \le n-2, \quad \mathcal{G} = \frac{1}{2\Delta}\{p_{i+1} - p_{i-1}\} + O(\Delta^2) \tag{19a}$$

$$\text{Boundary, } i = 2, \quad \mathcal{G} = \frac{1}{2\Delta}\{-p_{i+2} + 4p_{i+1} - 3p_i\} + O(\Delta^2) \tag{19b}$$

$$\text{Boundary, } i = n-1 \quad \mathcal{G} = \frac{1}{2\Delta}\{p_{i-2} - 4p_{i-1} + 3p_i\} + O(\Delta^2). \tag{19c}$$

Third-order forward-biased:

$$\text{Interior, } 3 \le i \le n-3, \quad \mathcal{G} = \frac{1}{6\Delta}\{-p_{i+2} + 6p_{i+1} - 3p_i - 2p_{i-1}\} + O(\Delta^3) \tag{20a}$$

$$\text{Boundary, } i = 2, \quad \mathcal{G} = \frac{1}{2\Delta}\{-p_{i+2} + 4p_{i+1} - 3p_i\} + O(\Delta^2) \tag{20b}$$

$$\text{Boundary, } i = n-1, \quad \mathcal{G} = \frac{1}{2\Delta}\{p_{i-2} - 4p_{i-1} + 3p_i\} + O(\Delta^2) \tag{20c}$$

$$\text{Boundary, } i = n-2, \quad \mathcal{G} = \frac{1}{6\Delta}\{p_{i-2} - 6p_{i-1} + 3p_i + 2p_{i+1}\} + O(\Delta^3). \tag{20d}$$

Fourth-order central-difference:

$$\text{Interior, } 4 \le i \le n-3, \quad \mathcal{G} = \frac{1}{12\Delta}\{-p_{i+2} + 8p_{i+1} - 8p_{i-1} + p_{i-2}\} + O(\Delta^4) \tag{21a}$$

$$\text{Boundary, } i = 2, \quad \mathcal{G} = \frac{1}{2\Delta}\{-p_{i+2} + 4p_{i+1} - 3p_i\} + O(\Delta^2) \tag{21b}$$

$$\text{Boundary, } i = 3, \quad \mathcal{G} = \frac{1}{2\Delta}\{p_{i+1} - p_{i-1}\} + O(\Delta^2) \tag{21c}$$

$$\text{Boundary, } i = n-2, \quad \mathcal{G} = \frac{1}{2\Delta}\{p_{i+1} - p_{i-1}\} + O(\Delta^2) \tag{21d}$$

$$\text{Boundary, } i = n-1, \quad \mathcal{G} = \frac{1}{2\Delta}\{p_{i-2} - 4p_{i-1} + 3p_i\} + O(\Delta^2). \tag{21e}$$

4.2. *The Interpolation Operator* ($\mathcal{I}$)

Two forms of the interpolation operator are investigated utilizing second- and fourth-order central-difference approximations. These operators are applied to the cell faces from $i = 3$ to $n - 1$. From Fig. 1, the cell faces denoted by $i = 2$ and $i = n$ coincide with the velocity nodes ($i = 1$ and n) and do not need to be interpolated. No special treatment is necessary at the boundaries for both cases, except with the fourth-order approximation at the boundary cell faces $i = 3$ and $n - 1$, the coefficients will be different due to the half cell at the boundaries.

Second-order central-difference:

$$\text{Interior, } 3 \le i \le n - 1, \qquad \mathcal{I} = \tfrac{1}{2}\{u_i + u_{i-1}\} \qquad + O(\Delta^2). \tag{22}$$

Fourth-order central-difference:

$$\text{Interior, } 3 \le i \le n - 1, \qquad \mathcal{I} = \tfrac{1}{16}\{-u_{i-2} + 9u_{i-1} + 9u_i - u_{i+1}\} \qquad + O(\Delta^4). \tag{23}$$

4.3. *The Laplacian Operator* ($\mathcal{L}$)

By using the gradient and interpolation operators with the divergence operator, different Laplacians are constructed. As an example, the Laplacian denoted by $\mathcal{L}_{43}$ is constructed by using a fourth-order approximation to the interpolation operator and a third-order forward-biased approximation to the gradient operator. Based on the above notation, six Laplacians are constructed and analyzed; $\mathcal{L}_{22}$, $\mathcal{L}_{23}$, $\mathcal{L}_{24}$, $\mathcal{L}_{42}$, $\mathcal{L}_{43}$, and $\mathcal{L}_{44}$. It should be noted that the analysis to follow is only performed on the interior approximation of the Laplacian for each case. The approximations at the boundaries, although necessary, do not contribute in any substantial way to the results presented. Table I summarizes the coefficients of the Laplacians.

Note in Table I that the coupling between nodes ($i - 1$, i, $i + 1$), which is absent in $\mathcal{L}_{22}$, is established in the other Laplacians. However, the forward-biased approximations of the gradient operator ($\mathcal{L}_{23}$ and $\mathcal{L}_{43}$) provide a much stronger coupling than the corresponding central-difference approximations. This observation is consistent with the Fourier analysis which will be shown later. But before that, it is useful to look at the difference between the $\mathcal{L}_{22}$ approximation and the other Laplacians. This is done by writing an expression of the type $\mathcal{L} = \mathcal{L}_{22} + \cdots$ in terms of the finite difference coefficients and then expanding these coefficients in a Taylor series approximation about i. The final expression can be written in the form

$$\begin{aligned}\mathcal{L} = \mathcal{L}_{22} &+ c_1 \Delta p_{xxx}|_i + c_2 \Delta^2 p_{xxxx}|_i \\ &+ c_3 \Delta^3 p_{xxxxx}|_i + c_4 \Delta^4 p_{xxxxxx}|_i + \cdots.\end{aligned} \tag{24}$$

Table II shows the first four coefficients of the expansion for the different Laplacians. For example, the Laplacian $\mathcal{L}_{23}$ is equivalent to the $\mathcal{L}_{22}$ Laplacian plus the addition of a fourth-derivative term as the leading term in the approximation. In all cases the fourth-order derivative term acts as a dissipation term of $O(\Delta^2)$ on the $\mathcal{L}_{22}$ operator and should help in damping out high frequency oscillations in the pressure field. In fact, Sotiropoulos and Abdallah [7] have used a form which is a subset of Eq. (24) for their Laplacian. They have added a fourth derivative term as artificial dissipation to damp out the pressure oscillations. Their (Eq. (27) in [7]) equivalent one-dimensional Laplacian is of the form

$$\mathcal{L}_{ss} = \mathcal{L}_{22} - \frac{\varepsilon}{4}\Delta^2 p_{xxxx}|_i, \tag{25}$$

where $0 \le \varepsilon \le 1$. For $\varepsilon = 1$, Eq. (25) is similar to the $\mathcal{L}_c$ Laplacian. For a two-dimensional driven cavity problem, they were able to obtain smooth pressure fields for a value of ε as low as 0.1. However, as a consequence of artificially adding the fourth-order dissipation term to the Laplacian $\mathcal{L}_{22}$ they are unable to satisfy discrete continuity exactly. Unlike [7], in the current formulation, the leading fourth-order derivative term is the outcome of using different approximations for the gradient and interpolation operator within a consistent framework which meets the conditions necessary to satisfy discrete continuity. In Table II, we also note that the Laplacians ($\mathcal{L}_{24}$, $\mathcal{L}_{42}$, and $\mathcal{L}_{44}$) constructed by using the central-difference approximations for the gradient operator are purely dissipative in their contribution to $\mathcal{L}_{22}$, while the $\mathcal{L}_{23}$ and $\mathcal{L}_{43}$ Laplacians also contribute a fifth-order derivative dispersive component of order $O(\Delta^3)$.

Figure 4 shows the results of a Fourier analysis on each of the Laplacians. For comparison, the compact Laplacians $\mathcal{L}_c$,

TABLE II

Coefficients of Taylor Series Expansion in Eq. (24) ($c_1 = 0$)

	c_2	c_3	c_4
$\mathcal{L}_{23}$	−1/6	−1/12	−5/72
$\mathcal{L}_{24}$	−1/6	0	−5/72
$\mathcal{L}_{42}$	−1/8	0	−5/96
$\mathcal{L}_{43}$	−7/24	−1/12	−29/288
$\mathcal{L}_{44}$	−7/24	0	−29/288

$\mathcal{L}_{22}$, and $\mathcal{L}_{sa}$ (for $\varepsilon = 0.1$ and 0.5) are also shown. All the Laplacians in Fig. 4 are bounded by $\mathcal{L}_{22}$ on the low side and $\mathcal{L}_c$ on the high side. One important observation made is that none of the Laplacians constructed in the present work resolve the grid scale ($\omega = \pi$). It is suspected that this is a consequence of the discrete form of the divergence operator used in the present work. A different form of the divergence operator (see Strikwerda and Nagel [10]) would be able to resolve the grid scale ($\omega = \pi$), but it would pose difficulties in satisfying discrete continuity. By the same token, $\mathcal{L}_{sa}$ does resolve the grid scales to varying degrees, depending on the value of ε, but it is unable to satisfy discrete continuity exactly. However, as we will see in the results presented, it is not always necessary to resolve the grid scale. It is found that merely increasing the accuracy of the Laplacian in the high wavenumber region goes a long way towards reducing, or in some cases eliminating, the pressure oscillations. In this respect, $\mathcal{L}_{23}$ and $\mathcal{L}_{43}$ are much better than $\mathcal{L}_{24}$, $\mathcal{L}_{42}$, and $\mathcal{L}_{44}$. Also from Fig. 4, almost all the Laplacians constructed in the present work show better accuracy than $\mathcal{L}_{sa}$ ($\varepsilon = 0.1$), except in the very high-wavenumber range. Based on the results of Sotiropoulos and Abdallah [7] for $\varepsilon = 0.1$, this would indicate that these Laplacians should work effectively towards reducing pressure oscillations.

5. RESULTS

The different Laplacians constructed were tested for a two-dimensional driven cavity problem (Ghia *et al.* [18]). The pressure field obtained is compared to a similar calculation on a staggered grid [17] with a $\mathcal{L}_c$ Laplacian. The number of calculation cells used were 16×16 and 32×32 for a Reynolds number of 1000. The unsteady equations were integrated in time until steady state was reached. Steady state was assumed when the absolute average change in the two velocity components from one time step to another was less than 1.E-10. In the current calculation, a direct LU factorization and inversion was used for the pressure–Poisson equation. Of course, for highly resolved flows and in three-dimensions, this is not possible and various other iterative techniques need to be used. As will be seen in the results presented it is sufficient to use the $\mathcal{L}_{23}$ Laplacian to greatly reduce the pressure oscillations (in this case, completely eliminate). This Laplacian has a six-point stencil in each direction and is diagonally dominant. Various iterative techniques can be employed in its solution. Line iterative techniques with multigrid acceleration can be employed with relaxation provided by penta-diagonal sweeps across the computational domain. Various Krylov subspace based methods like CGS [19], BICGSTAB [20], and GMRES [21] can also be applied. For domains with periodic boundaries, Fourier decomposition combined with iterative line sweeps for each wavenumber or combination of wavenumbers can be employed [22]. The use and implementation of any one of these methods will be dictated by the architecture, the boundary conditions, and the nature of the mass source term in the pressure–Poisson equation.

Figures 5a–f show line plots of the calculated pressure field on a 16×16 grid at $y = 0.5$, compared with that obtained with a staggered grid formulation. This location was chosen because it best exhibited the oscillations in the pressure field. The Laplacians formed from the central-difference gradient operators ($\mathcal{L}_{22}$, $\mathcal{L}_{24}$, $\mathcal{L}_{42}$, $\mathcal{L}_{44}$) clearly show the spurious oscillations in the pressure field. As expected the oscillations are strongest for the $\mathcal{L}_{22}$ Laplacian and are reduced for the $\mathcal{L}_{24}$ and $\mathcal{L}_{44}$ formulations. Again, as expected from the Fourier analysis, the best results are obtained by using the $\mathcal{L}_{23}$ and $\mathcal{L}_{43}$ Laplacians. For both Laplacians, the oscillations are damped out and the pressure distribution is smooth. Similar comparisons on a 32×32 grid are shown in Figs. 6a–f with similar results. For better clarity, the staggered grid pressure distribution ($\mathcal{L}_c$) is only shown in Fig. 6c. In addition, the pressure distribution obtained when a backward-biased gradient operator is used to construct the $\mathcal{L}_{23}$ Laplacian ($\mathcal{L}_{23b}$) is also shown in Fig. 6b. The pressure distributions for both are smooth with slight differences near the east boundary. Although not shown, discrete continuity is satisfied exactly in each computational cell for all of the formulations. The v-velocity obtained from the different formulations is compared to that obtained from a staggered grid formulation in Fig. 7. Figure 7a shows for comparison the data of Ghia *et al.* [18] for a 129×129 calculation. Figure 7b shows the velocity field obtained by both the $\mathcal{L}_{23}$ and $\mathcal{L}_{23b}$ Laplacians, which are indistinguishable from each other. It is found that the type of pressure formulation has very little effect on the prediction of the velocity field. Further, Figs. 6b and 7b testify to the insensitivity of the pressure and velocity field to the directional bias of the gradient operator. Although not evident from Fig. 7, since the $\mathcal{I}$ operator used in the formulation of the Laplacian is also used in the calculation of the convection term, the velocity field for the fourth-order $\mathcal{I}$ operator exhibits better accuracy than when the second-order interpolation operator is used.

6. CONCLUSIONS

In this study, the solution of the unsteady incompressible Navier–Stokes on a collocated grid is investigated. There are two counteracting problems in a collocated grid formulation: grid-scale pressure oscillations; the inability to satisfy discrete continuity exactly. Previous researchers (see [7], for instance) have found that often the solution to one of them often exacerbates the errors involved with the other. The main contribution of the present work is in developing a consistent formulation to construct the Laplacian in the pressure equation. It is shown that within this framework, Laplacians with different characteristics can be constructed, which satisfy discrete continuity and alleviate or eliminate the grid-scale pressure oscillations. The problem in satisfying discrete continuity is eliminated by using a second-order divergence operator applied over a finite-volume. The use of this divergence operator and the consistent treatment

of boundaries (similar to that on a staggered grid) satisfies the integrability constraint.

By using different approximations for the gradient operator and interpolation operator, six Laplacians with varying wavenumber characteristics are constructed. Fourier analyses and the application of these Laplacians to a driven cavity test problem show that a third-order forward- or backward-biased formulation of the gradient operator is successful in eliminating grid-scale pressure oscillations. Based on tests performed with the driven cavity problem, there was no observed sensitivity in the pressure and velocity fields to the directional bias of the gradient operator. Further tests are needed to assess these formulations in other flow fields.

REFERENCES

1. A. J. Chorin, *J. Comput. Phys.* **2,** 12 (1967).
2. S. Abdallah, *J. Comput. Phys.* **70,** 182 (1987).
3. A. J. Chorin, *Math. Comput.* **22,** 745 (1968).
4. S. V. Patankar, *Numerical Heat Transfer* (Hemisphere, Washington, DC/New York, 1980).
5. J. C. Strikwerda, *SIAM J. Sci. Stat. Comput.* **5**(1), 56 (1984).
6. K. Bube and J. C. Strikwerda, *SIAM J. Numer. Anal.* **20**(4), 653 (1983).
7. F. Sotiropoulos and S. Abdallah, *J. Comput. Phys.* **95,** 212 (1991).
8. S. W. Armfield, *Comput. Fluids* **20**(1), 1 (1991).
9. C. M. Rhie and W. L. Chow, *AIAA J.* **21**(11), (1983).
10. J. C. Strikwerda and Y. M. Nagel, *J. Comput. Phys.* **78,** 64 (1988).
11. F. M. Najjar and S. P. Vanka, "High-Order Formulation of the Pressure Poisson Equation on Collocated Finite-Difference Grids", Symposium for Advances in Computational Methods in Fluids, FED—Vol. 196, 1994 ASME Fluids Engineering Division Summer Meeting, Lake Tahoe, Nevada, June 1994, pp. 177–186.
12. S. W. Armfield, *Comput. Fluids* **20**(1), 1 (1991).
13. P. M. Gresho and R. L. Sani, *Int. J. Numer. Methods Fluids* **7,** 1111 (1987).
14. A. Arakawa, *J. Comput. Phys.* **1,** 119 (1966).
15. F. H. Harlow and J. E. Welch, *Phys. Fluids* **8**(12), 2182 (1965).
16. J. Kim and P. Moin, *J. Comput. Phys.* **59,** 308 (1985).
17. D. K. Tafti, *Int. J. Numer. Methods Fluids,* to appear.
18. U. Ghia, K. N. Ghia, and T. Shin, *J. Comput. Phys.* **48,** 387 (1982).
19. P. Sonneveld, *SIAM J. Sci. Statist. Comput.* **10,** 36 (1989).
20. H. A. Van Der Vorst, *SIAM J. Sci. Statist. Comput.* **13**(2) 631 (1992).
21. Y. Saad and M. H. Schultz, GMRES: *SIAM J. Sci. Statist. Comput.* **7,** 856 (1986).
22. D. K. Tafti, NCSA Technical Report P047, June 1994, to be presented at Seventh SIAM Conference on Parallel Processing for Scientific Computing, February 15–17, 1995 (unpublished).